Quaternary Science Reviews 267 (2021) 107105

Contents lists available at ScienceDirect

Quaternary Science Reviews

journal homepage: www.elsevier.com/locate/quascirev

Direct evidence for thinning and retreat of the southernmost Greenland ice sheet during the Younger Dryas

Anders E. Carlson [a, *], Alberto V. Reyes [b], Emily Gusterson [c], Yarrow Axford [d], Klaus M. Wilcken [e], Dylan H. Rood [c]

[a] Oregon Glaciers Institute, Corvallis, OR, 97330, USA
[b] Department of Earth and Atmospheric Sciences, University of Alberta, Edmonton, AB T6G 2E3, Canada
[c] Department of Earth Science and Engineering, Royal School of Mines, Imperial College London, SW7 2AZ, UK
[d] Department of Earth and Planetary Sciences, Northwestern University, Evanston, IL, 60208, USA
[e] Australian Nuclear Science and Technology Organization, New Illawarra Road, Lucas Heights, NSW, 2234, Australia

ARTICLE INFO

Article history:
Received 29 April 2021
Received in revised form
17 July 2021
Accepted 20 July 2021
Available online xxx

Handling Editor: C. O'Cofaigh

Keywords:
Pleistocene
Glaciation
Paleoclimatology
Greenland
Cosmogenic isotopes

ABSTRACT

During the last deglaciation, North Atlantic climate abruptly warmed at the Bølling (~14.7 ka), cooled into the Younger Dryas (~12.9 ka) and abruptly warmed again into the Holocene (~11.7 ka). While these events are defined by Greenland ice cores, there is still considerable uncertainty on Greenland ice-sheet margin responses to abrupt climate change. To refine the ice sheet's deglacial history, we present new cosmogenic nuclide surface exposure ages from boulders on bedrock at five sites in southernmost Greenland fjords located midway between the coast and inland ice margin. We find ice-sheet thinning below three local topographic highs at 12.7 ± 0.3 ka (n = 3), 13.1 ± 0.4 ka (n = 1, 2 outliers), and 12.3 ± 0.2 ka (n = 3), with up-fjord retreat at 12.5 ± 0.3 ka (n = 3) and 12.7 ± 0.2 ka (n = 4) based on two sites just above the mid-fjord marine limit. These mid-fjord ^{10}Be ages therefore show southernmost Greenland ice-sheet thinning and retreat during the Younger Dryas. We hypothesize that this thinning and retreat was a response to ocean warming prior to the Holocene and/or summer shortwave radiative forcing during the Younger Dryas due to peak boreal summer insolation. Our results also support a previously hypothesized winter bias in proxy records of Younger Dryas atmospheric cooling, since a large summer cooling during the Younger Dryas could have counteracted the effects of ocean warming and direct radiative forcing, inhibiting ice-sheet retreat.

1. Introduction

Greenland ice cores define the abrupt Bølling warming as occurring at ~14.7 ka with a ~14 °C increase in mean annual temperature, followed by the Younger Dryas cooling at ~12.9 ka of ~9 °C (Rasmussen et al., 2006; Buizert et al., 2014). The subsequent abrupt ~12 °C increase in mean annual temperature denotes the end of the Younger Dryas and onset of the Holocene at ~11.7 ka (Rasmussen et al., 2006; Buizert et al., 2014). Several studies have argued that the magnitudes of summer surface air temperature (SAT) changes over Greenland during these abrupt deglacial transitions were likely smaller than changes in mean annual air temperature, but few data constrain season-specific SAT changes during the Younger Dryas (Björck et al., 2002; Denton et al., 2005; Liu et al., 2012; Buizert et al., 2018). Furthermore, although these deglacial abrupt climate events are defined in Greenland ice-core proxies (Rasmussen et al., 2006), it remains unclear how the Greenland ice sheet's mass balance responded to these abrupt SAT changes. Marine records from west (Ó Cofaigh et al., 2013), south (Carlson et al., 2008) and southeast (Jennings et al., 2006) Greenland have been interpreted to paradoxically show increased ice-sheet mass loss and retreat during the Younger Dryas. Yet, terrestrial geologic evidence of Greenland ice-sheet fluctuations from this period is relatively sparse (Rinternknecht et al., 2014; Levy et al., 2016, 2020, 2020; Rainsley et al., 2018; Funder et al., 2021), because many sectors of the ice sheet did not retreat from the continental shelf onto land until the early Holocene (e.g., Bennike and Björck, 2002; Sinclair et al., 2016; Young et al., 2020, 2021; Funder et al., 2021).

However, a few parts of Greenland contain a terrestrial record of

* Corresponding author.
E-mail address: anders@orglaciersinst.org (A.E. Carlson).

https://doi.org/10.1016/j.quascirev.2021.107105
0277-3791/

ice-sheet extent prior to the Holocene (Bennike and Björck, 2002; Bennike et al., 2002; Larsen et al., 2011; Winsor et al., 2015; Sinclair et al., 2016; Levy et al., 2020; Funder et al., 2021). Based on cosmogenic nuclide surface exposure ages, southernmost Greenland's modern-day coastal landscapes began to deglaciate at 14.7 ± 0.5 ka (Fig. 1) (Levy et al., 2020) with ice reaching the inland late-Holocene ice margin at 11.0 ± 0.2 ka (Fig. 1) (Carlson et al., 2014; Nelson et al., 2014) (see Section 2 for age calculations). This early onset of deglaciation before the Younger Dryas is consistent with a minimum-limiting ^{14}C age of 13.9 ± 0.1 cal ka BP from an offshore island (Fig. 1) (Bennike et al., 2002; Björck et al., 2002). Another minimum-limiting ^{14}C age of 10.8 ± 0.2 cal ka BP from a lake near the modern ice-sheet margin indicates ice-free conditions far inland in the early Holocene (Fig. 1) (Larsen et al., 2011), which is supported by additional ^{14}C ages in between the coast and inland ice margin (Fig. 1) (Sparrenbom et al., 2006; Larsen et al., 2011). Collectively, ^{14}C and ^{10}Be evidence shows that southernmost Greenland contains a terrestrial record of ice-margin behavior from the Bølling onward. Yet there is currently little direct evidence for the ice sheet's behavior in this sector during the Younger Dryas itself.

Building on Larsen et al.'s (2011) inferences from minimum-limiting ^{14}C ages—mostly from Sparrenbom et al. (2006)—that date to the earliest Holocene (Fig. 1), Winsor et al. (2015) documented rapid deglacial retreat and thinning of the ice margin between Qaqortoq and Narsarsuaq in south Greenland. However, large (up to several kyr) analytical uncertainties on many of the study's ^{10}Be ages precluded determining the precise timing of ice-sheet thinning and retreat relative to abrupt climate changes including the Younger Dryas. More recently, Levy et al. (2020) dated the onset of coastal deglaciation around Greenland's southern tip, along with subsequent retreat inland within several small fjord systems, and inferred ice retreat during the Younger Dryas in the region outboard of today's Julianehåb ice cap. Likewise, Funder et al. (2021) used boulder and bedrock cosmogenic nuclide ages to document pre-Holocene coastal ice retreat in southwest Greenland from which they argued for ice-margin recession during the Younger Dryas. However, issues of potentially small degrees of nuclide inheritance (e.g., Young et al., 2021) precluded precisely relating ice-margin retreat to the timing of the Younger Dryas.

Here we refine our understanding of the Greenland ice-sheet response to deglacial abrupt climate change by synthesizing 16 new cosmogenic nuclide surface exposure ages from erratic boulders at five sites in southernmost Greenland across the mid-fjord region between ~70 m and ~810 m above modern sea level (Fig. 1). Combined with nine existing cosmogenic nuclide surface exposure ages, these new ages reveal ice-sheet thinning and retreat during the Younger Dryas, deep within the major fjords that channeled the southernmost Greenland ice sheet.

2. Methods

Cosmogenic nuclide surface exposure samples were collected from large boulders resting on bedrock. The sampling sites are located at multiple elevations across several fjords in a transect approximately perpendicular to ice-sheet flow (Figs. 1 and 3). At

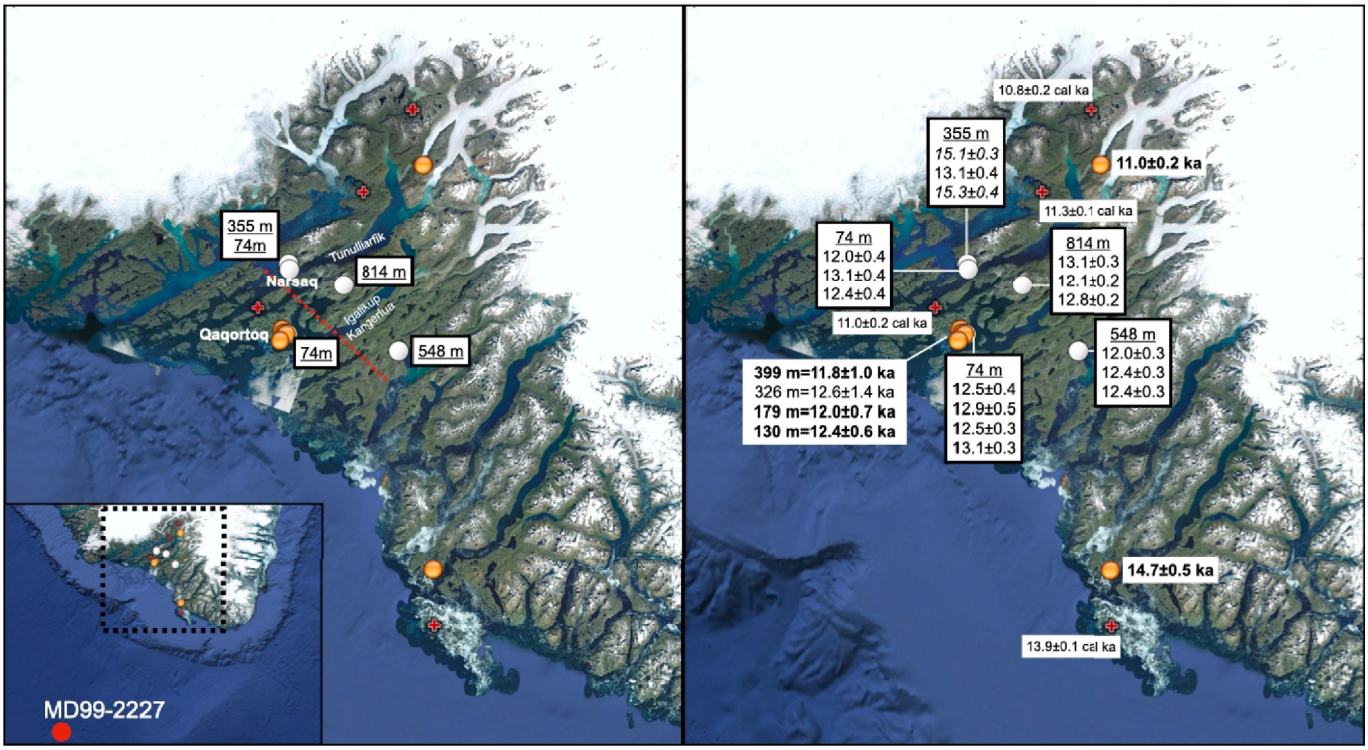

Fig. 1. Maps of the study region. Inset shows the location of the marine sediment records in Fig. 5 (red circle). Left shows the region with Narsaq, Qaqortoq and the two major fjords noted. Our ^{10}Be samples are shown by white circles with their average elevation noted. Yellow circles are previously published ^{10}Be boulder ages (Carlson et al., 2014; Nelson et al., 2014; Winsor et al., 2015; Levy et al., 2020) while red crosses are oldest minimum-limiting ^{14}C ages (Bennike et al., 2002; Sparrenbom et al., 2006; Larsen et al., 2011). Red dashed line is across-fjord transect shown in Fig. 3. Right is the same region but with our new ^{10}Be ages and analytical uncertainty listed in white boxes with black outlines; elevation of site noted. Italicized ages are samples considered to contain inherited ^{10}Be. Previously published ^{10}Be boulder ages have sample-set mean and uncertainty given in bold (or not in bold if an isolated age); elevation of site noted except for the coastal and inland sites. ^{14}C ages calibrated with Calib 8.2 (Stuiver et al., 2020) and IntCal2020 (Reimer et al., 2020). Images from Google Earth. (For interpretation of the references to colour in this figure legend, the reader is referred to the Web version of this article.)

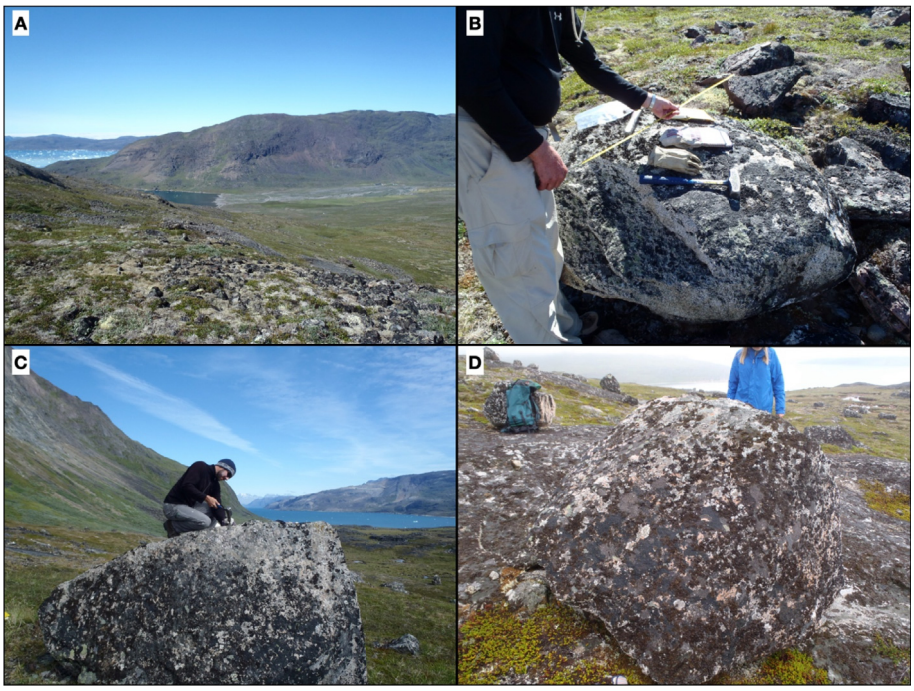

Fig. 2. Photographs of boulder samples and locations. (A) View towards fjord from the sample location of NQ13-04. (B) Sample NQ13-04 near Narsaq at 355 m asl. (C) Sample ND13-45 near Naraq just above the marine limit at 73 m asl. (D) Sample QQ13-01 near Qaqortoq just above the marine limit at 78 m asl.

three sites, flat, local topographic highs were chosen to avoid downslope movement of boulders after deglaciation (Fig. 2A and 2B, 3) (e.g., Winsor et al., 2015). ^{10}Be ages from these three sites thus date ice-sheet thinning below the local topography. The other two sites are located on flat bedrock just above the marine limit and thus date up-fjord ice-margin retreat (Fig. 2C and 2D, 3).

Going from the northwest to southeast (Fig. 1), we sampled three boulders resting on a local topographic bedrock high at ~360 m above modern sea level near the town of Narsaq (Fig. 2A and 2B, 3). Another three boulder samples on flat bedrock were collected near Narsaq from just above the marine limit at ~74 m above modern sea level (Figs. 2C and 3). Near Qaqortoq, four more boulders on flat bedrock were sampled just above the marine limit at ~74 m above modern sea level (Figs. 2D and 3). These Qaqortoq samples can be compared with those of Winsor et al. (2015) and Levy et al. (2020) from farther above the marine limit (Figs. 1 and 3). The highest sampling site has three boulders at ~810 m above modern sea level on a flat plateau southeast of Narsaq across the Tunulliarfik fjord and northeast of Qaqortoq (Figs. 1 and 3). Our fifth site, farther to the southeast across Igalikup Kangerlua fjord, consists of three more boulders on a flat summit at ~550 m (Figs. 1 and 3).

Quartz purification and cosmogenic ^{10}Be isotope dilution chemistry was conducted in the CosmIC Laboratories at Imperial College London using standard procedures (Corbett et al., 2016). The final purity of the quartz and beryllium, absence of native beryllium (i.e., ^{9}Be native to the quartz mineral separate, rather than added as carrier), and high yield of beryllium were all verified using an Agilent 5100 SVDV ICP-OES. Beryllium oxide was mixed with niobium in a 1:1 M ratio and packed into copper cathodes for ^{10}Be/^{9}Be isotopic analysis by accelerator mass spectrometry on the 6 MV Sirius tandem accelerator in the Centre for Accelerator Science at ANSTO (Wilcken et al., 2017). Data were normalized to the KN-5-3 standard with a reported ^{10}Be/^{9}Be ratio of 6.32×10^{-12}, which is consistent with the revised ^{10}Be decay constant (Nishiizumi et al., 2007). Secondary standards produced by K. Nishiizumi were run as unknowns to confirm the linearity of the isotopic measurements. A full process blank (Be carrier only) was processed with each batch of samples. The total ^{10}Be atoms measured in the blank for each batch was subtracted from the total ^{10}Be atoms measured in the samples in that batch with uncertainties in sample and batch-specific blank propagated in quadrature. The ^{10}Be/^{9}Be blank ratios represent a small portion (0.8–8.2 %) of the measured sample isotopic ratios. Isotopic ratio data were reduced to isotope concentrations considering the background-corrected isotopic ratios, the mass of quartz dissolved, and the total ^{9}Be carrier added to the sample. All sample ^{10}Be information is contained in Table 1 and S1.

All new and existing ^{10}Be ages were calculated using the Arctic production rate of Young et al. (2013) and the Lal/Stone time-dependent scaling (Balco et al., 2008). We utilize only ^{10}Be ages from prior studies with <20 % analytical uncertainty, which excludes four of the ten ^{10}Be ages from Winsor et al. (2015) at Qaqortoq. Application of Chauvenet's criterion did not flag any statistical outliers. We calculated mean square weighted deviation (MSWD) for each group of ^{10}Be dates at a site to identify the appropriate method of calculating the sample mean and uncertainty: we use the arithmetic mean and standard error for MSWD >1, and the inverse-error-weighted mean and uncertainty for MSWD <1 (Cuzzone et al., 2016; Ullman et al., 2016). In so doing, we maximize the uncertainty of the mean, making this a conservative approach to estimating the true timing of deglaciation. In one instance in the dataset from Winsor et al. (2015), only two samples were available at a location (Fig. 4); we thus calculate their arithmetic mean, with their analytical uncertainty added in quadrature. We do not include a correction for isostatic uplift on boulder age as this effect is likely to be quite small, given the marine limit of only ~35 m in the region (Sparrenbom et al., 2006; Carlson, 2020).

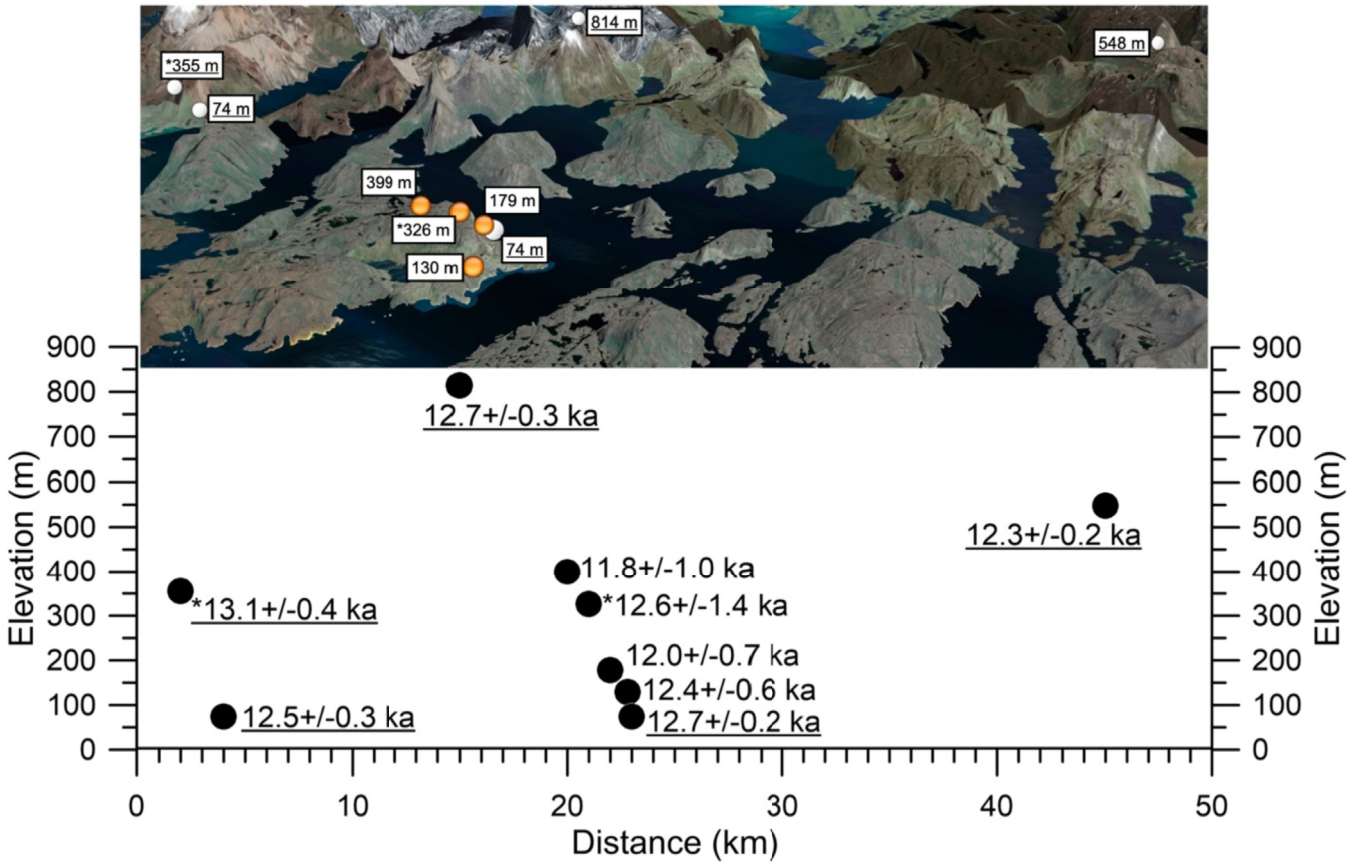

Fig. 3. Spatial distribution of sampling sites and ^{10}Be ages along perpendicular-to-flow mid-fjord transect. Top is an oblique image looking northeast from Google Earth with 3-times vertical exaggeration. White circles are our sampling sites; yellow circles are existing ^{10}Be ages. Elevation of the site is noted with underlined indicating our site; an asterisk indicates a single ^{10}Be age at that site. Bottom shows sample site elevation versus distance projected onto the across-fjord transect (red dashed line in Fig. 1). Site mean and uncertainty indicated with underlined ages indicating our new data; asterisk indicates individual sample age with analytical uncertainty. (For interpretation of the references to colour in this figure legend, the reader is referred to the Web version of this article.)

Table 1
^{10}Be sample information. Ages were calculated assuming a density of 2.65 g cm^{-3} and standard atmosphere.

Sample Name	Latitude	Longitude	Elevation (m)	Thickness (cm)	Shielding	[^{10}Be] (at/g)	Uncert. (at/g)	Age(ka)	Uncert. (ka)
NQ-13-03	60.9200	-46.0236	366	2.0	0.9807	92385	1994	15.1	0.3
NQ-13-04	60.9205	-46.0229	355	2.0	0.9881	77428	2359	13.1	0.4
NQ-13-06	60.9217	-46.0286	353	2.0	0.9923	93355	2140	15.3	0.4
NQ-13-43	60.9063	-46.0207	73	2.0	0.9697	53941	1836	12.0	0.4
NQ-13-44	60.9065	-46.0209	75	3.0	0.9610	57940	1923	13.1	0.5
NQ-13-45	60.9068	-46.0200	73	2.0	0.9738	56021	1954	12.4	0.5
NH-16-1	60.8682	-45.7174	803	2.0	0.9797	119189	2405	13.1	0.3
NH-16-3	60.8687	-45.7176	803	2.0	0.9750	109729	2221	12.1	0.2
NH-16-5	60.8651	-45.7260	836	2.0	0.9764	119202	2164	12.8	0.2
PC-16-1	60.6970	-45.4057	526	2.0	0.9259	80634	2047	12.0	0.3
PC-16-2	60.6955	-45.4060	551	2.0	0.9633	88653	1973	12.4	0.3
PC-16-3	60.6952	-45.4065	567	2.0	0.9839	91933	2143	12.4	0.3
QQ-13-01	60.7320	-46.0163	78	2.5	0.9885	57329	1644	12.5	0.4
QQ-13-02	60.7319	-46.0157	72	2.0	0.9885	59263	2095	12.9	0.5
QQ-13-03	60.7319	-46.0157	72	2.5	0.9885	56972	1450	12.5	0.3
QQ-13-04	60.7324	-46.0152	74	1.5	0.9885	60320	1536	13.1	0.3

3. Results

Our highest-elevation sampling location at 803–836 m above modern sea level has an arithmetic mean and standard error of 12.7 ± 0.3 ka (n = 3; MSWD = 3.9) (Figs. 3 and 4), indicating ice-sheet thinning below this summit. The next lower and southernmost sampling location at 526–567 m has an error-weighted mean and uncertainty of 12.3 ± 0.2 ka (n = 3; MSWD = 0.7) (Figs. 3 and 4), also showing ice-sheet thinning at this time. The three boulders from 353 to 366 m near Narsaq have ages of 15.3 ± 0.4 ka, 15.1 ± 0.3 ka and 13.1 ± 0.4 ka (Fig. 4A). Based on all the other ^{10}Be surface exposure ages in the region and laws of geomorphic superposition, we suggest that the two samples older than ~15 ka contain slight inheritance and only utilize the youngest age of 13.1 ± 0.4 ka when

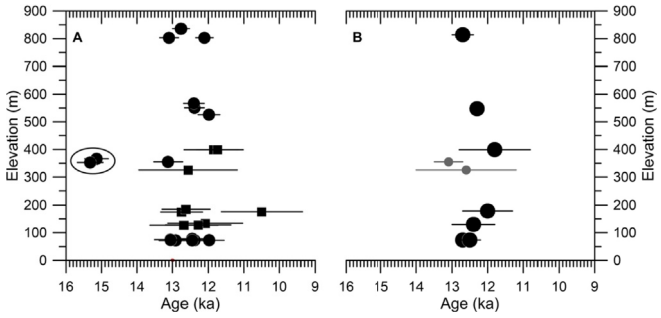

Fig. 4. Mid-fjord ^{10}Be ages. (A) Elevation-age plot for new (circles) and existing (squares)^{10}Be. Black oval indicates the two samples considered to contain inheritance. (B) Mean and uncertainty for each ^{10}Be age site shown by black circles; two gray symbols are individual ^{10}Be ages with analytical uncertainty.

interpreting the deglacial history of the region (Figs. 3 and 4B). Young et al. (2020) made a similar superposition argument to identify slight amounts of inheritance in the coastal ^{10}Be samples near Sisimiut of Winsor et al. (2015). At our lowest elevation sites, we date up-fjord ice retreat from 73 to 75 m above modern sea level near Narsaq at 12.5 ± 0.3 ka (n = 3; MSWD = 1.6, arithmetic mean and standard error) and from 72 to 78 m near Qaqortoq at 12.7 ± 0.2 ka (n = 4; MSWD = 0.8, error-weighted mean and uncertainty) (Figs. 3 and 4).

4. Discussion

Our new ^{10}Be ages are consistent with the existing ^{10}Be and ^{14}C deglacial chronology for the region (Figs. 1, 3 and 4). There is excellent agreement between the new ^{10}Be ages just above the marine limit at Qaqortoq (12.7 ± 0.2 ka) and those of Levy et al. (2020) at ~130 m above modern sea level of 12.4 ± 0.6 ka (n = 3; MSWD = 0.1, error-weighted mean and uncertainty). The new ^{10}Be ages also corroborate the deglacial chronology of Winsor et al. (2015) near Qaqortoq, who dated ice-margin thinning through ~400 m at 11.8 ± 1.0 ka (n = 2), through ~330 m at 12.6 ± 1.4 ka (n = 1), and through ~180 m at 12.0 ± 0.7 ka (n = 3; MSWD = 1.6, arithmetic mean and standard error). Likewise, our timings of mid-fjord deglaciation in southernmost Greenland of 12.7 ± 0.2 ka near Qaqortoq and 12.5 ± 0.3 ka near Narsaq are compatible with an adjacent minimum-limiting ^{14}C deglaciation age of 11.0 ± 0.2 ka and another minimum-limiting ^{14}C date of 11.3 ± 0.2 ka closer to the fjord head (Fig. 1) (Sparrenbom et al., 2006).

The lack of major deglacial moraines in the region (Weidick, 1963; Larsen et al., 2011) makes it difficult to define deglacial ice-margin locations. However, it is possible to estimate the broad timing of ice retreat from the outer coast to the mid-fjord and, in turn, to near the inland late-Holocene margin. Levy et al. (2020) dated coastal deglaciation to 14.7 ± 0.5 ka (n = 3; MSWD = 0.6, error-weighted mean and uncertainty) (Fig. 1). We show continued ice-margin retreat with mid-fjord deglaciation at 12.5 ± 0.3 ka near Narsaq and at 12.7 ± 0.2 ka near Qaqortoq. The ice-sheet margin then reached its late-Holocene ice limit by 11.0 ± 0.2 ka (n = 6; MSWD = 1.9, arithmetic mean and uncertainty) (Fig. 1; Carlson et al., 2014; Nelson et al., 2014).

The new ^{10}Be exposure ages from this region provide the first clear and direct evidence for ice-sheet thinning and subsequent ice-sheet-margin retreat during the Younger Dryas (Fig. 5A), which is consistent with the existing ^{10}Be and ^{14}C chronology for the region (Sparrenbom et al., 2006; Larsen et al., 2011; Winsor et al., 2015; Levy et al., 2020) and the lack of mid-fjord moraines (Weidick, 1963; Larsen et al., 2011). Indeed, on the Eirik Drift off south Greenland (Fig. 1), geochemical proxies in sediment core MD99-2227 suggest increased delivery of terrigenous sediment due to ablation-driven runoff from the southern Greenland ice sheet during the Younger Dryas (Fig. 5B) (Carlson et al., 2008), while Earth models constrained by relative sea-level data simulate southernmost Greenland deglaciation occurring 14-12 ka (Bennike et al., 2002). Our results add to a growing number of studies that reconstruct seemingly paradoxical ice-sheet retreat during the Younger Dryas elsewhere in Greenland (e.g., Jennings et al., 2006; Carlson et al., 2008; Ó Cofaigh et al., 2013; Rinternknecht et al., 2014; Levy et al., 2016, 2020; Rainsley et al., 2018; Funder et al., 2021), despite ice-core evidence for dramatic cooling over central to southern Greenland (Buizert et al., 2014, 2018) at this time. There is now particular convergence of evidence for Younger Dryas ice-margin retreat in southernmost Greenland (Carlson et al., 2008; Larsen et al., 2011; Winsor et al., 2015; Levy et al., 2020; Funder et al., 2021).

Notably, the Younger Dryas may have been characterized by extreme seasonality in SAT, meaning that the ice-core paleoclimate proxies are dominated by a strong winter cooling signal (Liu et al., 2012). Almost two decades ago, Björck et al. (2002) reported qualitative paleoecological evidence that southernmost Greenland summers were mild during the Younger Dryas, alongside evidence from the same site for very cold Younger Dryas winters. Denton et al. (2005) contrasted limited snowline lowering in East Greenland during the Younger Dryas with the intense cooling documented in ice cores over central Greenland and suggested that increased seasonality might explain that apparent conundrum. Climate models support greater seasonality of SATs over Greenland during the Younger Dryas (Fig. 5C) (Liu et al., 2012) and have facilitated estimates of summer SAT based on deconvolving annual-mean ice-core temperatures (Buizert et al., 2018). However, this latter approach still suggests that Younger Dryas summer SAT was >4.5 °C cooler than during the preceding Allerød interval (Fig. 5C) and only ~2 °C warmer than during the last glacial maximum. To date, there are no quantitative proxy datasets that directly record summer SAT in Greenland during the Younger Dryas, so estimates of summer conditions, and thus of SAT-driven changes in ice-sheet surface mass balance during the Younger Dryas, remain highly uncertain.

We suggest that oceanic warming and the direct effects of rising boreal summer insolation on ice-sheet surface mass balance may have together counteracted any summer SAT cooling and caused the thinning and retreat of the ice sheet in southernmost Greenland (Jennings et al., 2006; Winsor et al., 2012, 2015, 2015; Sinclair et al., 2016; Rainsley et al., 2018; Levy et al., 2020; Funder et al., 2021). Importantly, adjacent Labrador Sea surface and subsurface temperatures warmed from glacial to Holocene levels during the Younger Dryas (Figs. 1 and 5D) (Solignac et al., 2004; Winsor et al., 2012). Warming ocean waters could have promoted accelerated submarine melt of marine-terminating ice margins in southernmost Greenland fjords (Fig. 1), driving ice-margin thinning and

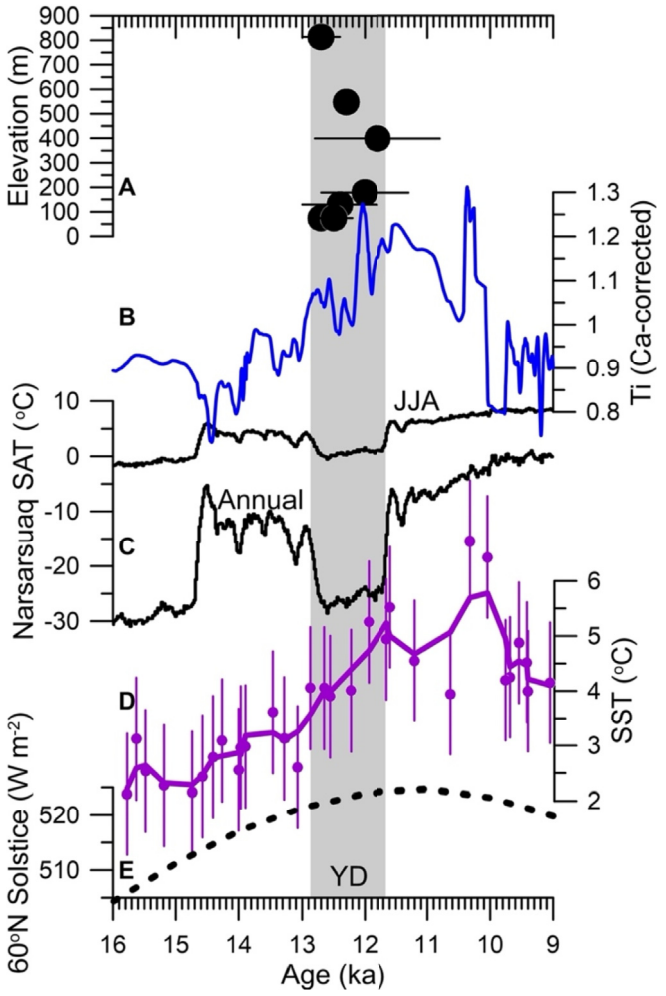

Fig. 5. Last deglaciation of southernmost Greenland and its potential climate forcings. (A) Elevation-age plot for mid-fjord mean ^{10}Be ages (black circles; individual ages excluded) (red dashed line in Fig. 1). (B) Southern Greenland ice-sheet runoff proxy: Ca-corrected Ti concentration from MD99-2227 (Fig. 1) (Carlson et al., 2008). (C) Summer (June, July, August; JJA) and annual SAT deconvolved for southernmost Greenland (60.5°N, 45.0°W, ~410 m asl) from ice-core annual SAT and climate-model seasonality (Buizert et al., 2018). (D) MD99-2227 Mg/Ca SST from the Labrador Sea (symbols; Fig. 1) with three-point smoothing (line) (Winsor et al., 2012). (E) Solstice boreal summer insolation (Laskar et al., 2004). Gray vertical bar denotes the Younger Dryas (YD; Rasmussen et al., 2006). (For interpretation of the references to colour in this figure legend, the reader is referred to the Web version of this article.)

retreat (e.g., Rignot et al., 2010, 2015; Straneo and Heimbach, 2013). Local summer insolation also reached its maximum by the end of the Younger Dryas (Fig. 5E). Because shortwave radiation accounts for a large fraction of summer ablation on the modern Greenland ice sheet (e.g., Braithwaite, 1995; Ettema et al., 2009), elevated boreal summer insolation may have been sufficient to continue surface ablation even if and where summer SAT fell to near freezing during the Younger Dryas (Fig. 5C).

5. Conclusions

We add to the deglacial history of the southernmost Greenland ice sheet using new ^{10}Be surface exposure ages from the mid-fjord region that directly record ice-sheet thinning and retreat during the Younger Dryas. Though resolution of the apparent conundrum between thinning and retreat at a time of climate cooling awaits direct proxies for seasonal SAT reconstruction, concurrent ocean warming and rising boreal insolation may have offset any summer SAT cooling during the Younger Dryas, in turn driving retreat of the southernmost Greenland ice sheet.

Data availability

All data presented in this paper are available in Table 1 and S1.

Author contributions

Anders Carlson and Alberto Reyes conceived of the study and conducted the majority of the fieldwork. Emily Gusterson, Klaus Wilcken and Dylan Rood performed the chemical separation, AMS analyses and data processing. Yarrow Axford compiled paleoclimate records for the Younger Dryas period in southern Greenland. All authors contributed to interpretation of the data and writing of the manuscript.

Declaration of competing interest

The authors declare that they have no known competing financial interests or personal relationships that could have appeared to influence the work reported in this paper.

Acknowledgements

We thank the people and Government of Greenland for permission to conduct field work on the island and Gaylen Sinclair for leading fieldwork that collected some of the samples presented here. Allan C. Carlson, Elizabeth C.B. Carlson, Aaron Hartz, G. Everett Lasher, Jamie McFarlin, and CH2M Hill Polar Field Services provided help in the field. Alex Seal aided with laboratory chemistry. Comments from two anonymous reviewers substantially improved this manuscript.

Funding

This work was supported by U.S. National Science Foundation [1557541, 1454734, 2002515], the Australian Nuclear Science Technology Organization (ANSTO) for Research Portal Proposal [AP11292], and the Australian Government for the Centre for Accelerator Science at ANSTO through the National Collaborative Research Infrastructure Strategy (NCRIS).

Appendix A. Supplementary data

Supplementary data to this article can be found online at https://doi.org/10.1016/j.quascirev.2021.107105.

References

Balco, G., Stone, J.O., Lifton, N.A., Dunai, T.J., 2008. A complete and easily accessible means of calculating surface exposure ages or erosion rates from 10Be and 26Al measurements. Quat. Geochronol. 3, 174–195.
Bennike, O., Björck, S., 2002. Chronology of the last recession of the Greenland ice sheet. J. Quat. Sci. 17, 211–219.
Bennike, O., Björck, S., Lambeck, K., 2002. Estimates of South Greenland late-glacial ice limits from a new relative sea level curve. Earth Planet Sci. Lett. 197, 171–186.
Björck, S., Bennike, O., Rosén, P., Andresen, C.S., Bohncke, S., Kaas, E., Conley, D., 2002. Anomalously mild Younger Dryas summer conditions in southern Greenland. Geology 30, 427–430.
Braithwaite, R.J., 1995. Positive degree-day factors for ablation on the Greenland ice sheet studied by energy-balance modelling. J. Glaciol. 41, 153–160.
Buizert, C., Gkinis, V., Severinghaus, J.P., He, F., Lecavalier, B.S., Kindler, P., Leuenberger, M., Carlson, A.E., Vinther, B., Masson-Delmotte, V., White, J.W.C., Liu, Z., Otto-Bliesner, B., Brook, E.J., 2014. Greenland temperature response to climate forcing during the last deglaciation. Science 345, 1177–1180.
Buizert, C., Keisling, B.A., Box, J.E., He, F., Carlson, A.E., Sinclair, G., DeConto, R.M.,

2018. Greenland-wide seasonal temperatures during the last deglaciation. Geophys. Res. Lett. https://doi.org/10.1002/2017GL075601.
Carlson, A.E., 2020. Comment on: deglaciation of the Greenland and Laurentide ice sheets interrupted by glacier advance during abrupt coolings. Quat. Sci. Rev. 240, 106354.
Carlson, A.E., Stoner, J.S., Donnelly, J.P., Hillaire-Marcel, C., 2008. Response of the southern Greenland Ice Sheet during the last two deglaciations. Geology 36, 359–362.
Carlson, A.E., Winsor, K., Ullman, D.J., Brook, E.J., Rood, D.H., Axford, Y., LeGrande, A.N., Anslow, F.S., Sinclair, G., 2014. Earliest Holocene south Greenland ice-sheet retreat within its late-Holocene extent. Geophys. Res. Lett. 41, 5514–5521.
Corbett, L.B., Bierman, P.R., Rood, D.H., 2016. Constraining multi-stage exposure-burial scenarios for boulders preserved beneath cold-based glacial ice in Thule, northwest Greenland. Earth Planet Sci. Lett. 440, 147–157.
Cuzzone, J.K., Clark, P.U., Carlson, A.E., Ullman, D.J., Rinterknecht, V.R., Milne, G.A., Lunkka, J.-P., Wohlfarth, B., Marcott, S.A., Caffee, M., 2016. Final deglaciation of the Scandinavian Ice Sheet and implications for the Holocene global sea-level budget. Earth Planet Sci. Lett. 448, 34–41.
Denton, G.H., Alley, R.B., Comer, G.C., Broecker, W.S., 2005. The role of seasonality in abrupt climate change. Quat. Sci. Rev. 24, 1159–1182.
Ettema, J., van den Broeke, M.R., van Meijgaard, E., van de Berg, W.J., Bamber, J.L., Box, J.E., Bales, R.C., 2009. Higher surface mass balance of the Greenland ice sheet revealed by high-resolution climate modeling. Geophys. Res. Lett. 36. https://doi.org/10.1029/2009GL038110.
Funder, S., Sørensen, A.H.L., Larsen, N.K., Bjørk, A.A., Briner, J.P., Olsen, J., Schomacker, A., Levy, L.B., Kjær, K.H., 2021. Younger Dryas ice margin retreat in Greenland: new evidence from southwestern Greenland. Clim. Past 17, 587–601.
Jennings, A.E., Hald, M., Smith, M., Andrews, J.T., 2006. Freshwater forcing from the Greenland Ice Sheet during the Younger Dryas: evidence from southeastern Greenland shelf cores. Quat. Sci. Rev. 25, 282–298.
Larsen, N.K., Kjær, K.H., Olsen, J., Funder, S., Kjeldsen, K.K., Nørgaard-Pedersen, 2011. Restricted impact of Holocene climate variations on the southern Greenland Ice Sheet. Quat. Sci. Rev. 30, 3171–3180.
Laskar, J., Robutel, P., Joutel, F., Gastineau, M., Correia, A.C.M., Levrard, B., 2004. A long-term numerical solution for the insolation quantities of the Earth. A&A 428, 261–285.
Levy, L.B., Kelly, M.A., Lowell, T.V., Hall, B.L., Howley, J.A., Smith, C.A., 2016. Coeval fluctuations of the Greenland ice sheet and a local glacier, central East Greenland, during late glacial and early Holocene time. Geophys. Res. Lett. 43, 1623–1631.
Levy, L.B., Larsen, N.K., Knudsen, M.F., Egholm, D.L., Bjørk, A.A., Kjeldsen, K.K., Kelly, M.A., Howley, J.A., Olsen, J., Tikhomirov, D., Zimmerman, S.R.H., Kjær, K.H., 2020. Multi-phased deglaciation of south and southeast Greenland controlled by climate and topographic setting. Quat. Sci. Rev. 242, 106454.
Liu, Z., Carlson, A.E., He, F., Brady, E.C., Otto-Bliesner, B.L., Briegleb, B.P., Wehrenberg, M., Clark, P.U., Wu, S., Cheng, J., Zhang, J., Noone, D., Zhu, J., 2012. Younger Dryas cooling and the Greenland climate response to CO_2. Proc. Natl. Acad. Sci. Unit. States Am. 109, 11101–11104.
Nelson, A.H., Bierman, P.R., Shakun, J.D., Rood, D.H., 2014. Using *in situ* cosmogenic 10Be to identify the source of sediment leaving Greenland. Earth Surf. Process. Landforms 39, 1087–1100.
Ó Cofaigh, C., Dowdeswell, J.A., Jennings, A.E., Hogan, K.A., Kilfeather, A., Hiemstra, J.F., Noormets, R., Evans, J., McCarthy, D.J., Andrews, J.T., Lloyd, J.M., Moros, M., 2013. An extensive and dynamic ice sheet on the West Greenland shelf during the last glacial cycle. Geology 41, 219–222.
Rainsley, E., Menviel, L., Fogwill, C.J., Turney, C.S.M., Hughes, A.L.C., Rood, D.H., 2018. Greenland ice mass loss during the younger Dryas driven by Atlantic meridional overturning circulation feedbacks. Sci. Rep. 8. https://doi.org/10.1038/s41598-018-29226-8.
Rasmussen, S.O., Anderson, K.K., Svensson, A.M., Steffensen, J.P., Vinther, B.M., Clausen, H.B., Siggaard-Andersen, M.-L., Johnsen, S.J., Larsen, L.B., Dahl-Jensen, D., Bigler, M., Röthlisberger, R., Fischer, H., Goto-Azuma, K., Hansson, M.E., Ruth, U., 2006. A new Greenland ice core chronology for the last glacial termination. J. Geophys. Res. 111, D06102.
41 co-authors Reimer, P.J., 2020. The IntCal20 northern hemisphere radiocarbon age calibration curve (0–55 cal kBP). Radiocarbon 62, 725–757.
Rignot, E., Koppes, M., Velicogna, I., 2010. Rapid submarine melting of the calving faces of West Greenland glaciers. Nat. Geosci. 3, 187–191.
Rignot, E., Fenty, I., Xu, Y., Cai, C., Kemp, C., 2015. Undercutting of marine-terminating glaciers in West Greenland. Geophys. Res. Lett. 42, 5909–5917.
Rinterknecht, V., Jomelli, V., Brunstein, D., Favier, V., Masson-Delmotte, V., Bourlès, D., Leanni, L., Schläppy, R., 2014. Unstable ice stream in Greenland during the Younger Dryas cold event. Geology 42, 759–762.
Sinclair, G., Carlson, A.E., Mix, C.A., Lecavalier, B., Milne, G., Matthias, A., Buizert, C., DeConto, R., 2016. Diachronous retreat of the Greenland ice sheet during the last deglaciation. Quat. Sci. Rev. 145, 243–258.
Solignac, S., de Vernal, A., Hillaire-Marcel, C., 2004. Holocene sea-surface conditions in the North Atlantic – contrasted trends and regimes in the western and eastern sectors (Labrador Sea vs. Iceland Basin). Quat. Sci. Rev. 23, 319–334.
Sparrenbom, C.J., Bennike, O., Björck, S., Lambeck, K., 2006. Holocene relative sea-level changes in the Qaqortoq area, southern Greenland. Boreas 35, 171–187.
Straneo, F., Heimbach, P., 2013. North Atlantic warming and the retret of Greeland's outlet glaciers. Nature 504, 36–43.
Stuiver, M., Reimer, P.J., Reimer, R.W., 2020. CALIB 8.2 [WWW program]. http://calib.org. accessed 2020-9-16.
Ullman, D.J., Carlson, A.E., Hostetler, S.W., Clark, P.U., Cuzzone, J., Milne, G.A., Winsor, K., Caffee, M., 2016. Final Laurentide ice-sheet deglaciation and Holocene climate-sea level change. Quat. Sci. Rev. 152, 49–59.
Weidick, A., 1963. Ice margin features in the Julianehab District. Meddelelser Om Grønland 165, 1–133.
Winsor, K., Carlson, A.E., Caffee, M., Rood, D.H., 2015. Rapid last-deglacial thinning and retreat of the marine-terminating southwestern Greenland ice sheet. Earth Planet Sci. Lett. 426, 1–12.
Winsor, K., Carlson, A.E., Klinkhammer, G.P., Stoner, J.S., Hatfield, R.H., 2012. Evolution of the northeast Labrador Sea during the last interglaciation. Geochem., Geophys., Geosys. 13. https://doi.org/10.1029/2012GC004263.
Young, N.E., Schaefer, J.M., Briner, J.P., Goehring, B.M., 2013. A Be-10 production-rate calibration for the Arctic. J. Quat. Sci. 28, 515–526.
Young, N.E., Briner, J.P., Miller, G.H., Lesnek, A.J., Crump, S.E., Thomas, E.K., Pendleton, S.L., Cuzzone, J., Lamp, J., Zimmerman, S., Caffee, M., Schaefer, J.M., 2020. Deglaciation of the Greenland and Laurentide ice sheets interrupted by glacier advance during abrupt coolings. Quat. Sci. Lett. 229, 106091.
Young, N.E., Lesnek, A.J., Cuzzone, J.K., Briner, J.P., Badgeley, J.A., Balter-Kennedy, A., Graham, B.L., Cluett, A., Lamp, J.L., Schwartz, R., Tuna, T., Bard, E., Caffee, M.W., Zimmerman, S.R.H., Schaefer, J.M., 2021. In situ cosmogenic 10Be-14C-26Al measurements from recently deglaciated bedrock as a new tool to decipher changes in Greenland Ice Sheet size. Clim. Past 17, 419–450.